Chaiyo *et al. Micro and Nano Systems Letters* (2025) 13:31
https://doi.org/10.1186/s40486-025-00247-z

Micro and Nano Systems Letters

CORRESPONDENCE Open Access

Low-cost domestic microwave synthesis of SnO_2/CuO nanostructure for ethanol detection

Pitchanunt Chaiyo[1†], Mohamed Ahmed Belal[2†], Sugato Hajra[3], Swati Panda[3], Premkumar Sharad Bhosale[2], Hohyun Keum[4,5*] and Hoe Joon Kim[2*]

Abstract

Low-cost preparation of nanostructured materials is one of the important factors for the commercialization of sensors. This study reports the sustainable and low-cost synthesis of pure SnO_2 and SnO_2-CuO nanostructures using a domestic microwave annealing approach. The material obtained was structurally examined using X-ray diffraction and a scanning electron microscope. The pure SnO_2 and SnO_2-CuO inks were deposited over laser-induced graphene interdigitated electrodes. Towards the volatile organic compounds, the pure SnO_2 and SnO_2-CuO went through ethanol sensing. The SnO_2-CuO-based sensor demonstrated strong response and selectivity for detecting ethanol at room temperature with a response of 11%, a response time of 53 s, and a recovery time of 64 s at 100 ppm of ethanol. The high response and selectivity of the sensor towards ethanol make it ideal for continuous tracking in both environmental and industrial settings.

Keywords Ethanol, VOC gases, Spray coating, Pure SnO_2 and SnO_2-CuO, LIG

Introduction

Today's world has experienced continuous economic and industrial development, leading to the production and emission of various gases. Some of these gases are beneficial, while others harm human health [1–3]. These gases are categorized into inorganic and volatile organic compounds (VOCs) [4, 5]. Therefore, it is necessary to develop gas detection devices to identify toxic and flammable gases that may leak into the air [6]. These devices are essential for protecting people in high-risk workplaces and the environment. The metal oxide materials, such as tin dioxide (SnO_2) and copper oxide (CuO), are widely used in gas detection [7]. This is due to their high response, low cost [8], semiconductive behavior, and high lifetime stability [9]. SnO_2 is an n-type semiconductor with a large bandgap of 3.6 eV at room temperature (RT) [9]. SnO_2 has different morphological structures, including thin films, composite materials, and porous

†Pitchanunt Chaiyo and Mohamed Ahmed Belal have contributed equally to this work.

*Correspondence:
Hohyun Keum
hkeum@kitech.re.kr
Hoe Joon Kim
joonkim@dgist.ac.kr
[1]Faculty of Sports and Health Science, National Sports University Sisaket Campus, Sisaket 33000, Thailand
[2]Department of Robotics and Mechatronics Engineering, Daegu Gyeongbuk Institute of Science & Technology (DGIST), Daegu 42988, Korea
[3]Department of Electrical Engineering and Computer Science, Daegu Gyeongbuk Institute of Science & Technology (DGIST), Daegu 42988, Korea
[4]Department of Mechanical Engineering, Chung-Ang University, Seoul 06974, Republic of Korea
[5]Industrial Transformation Technology Department, Korea Institute of Industrial Technology, Cheaonan-si 31056, Republic of Korea

nanofibers [10], and nanoparticles that can be used in gas detector applications. On the other hand, CuO has different advantages, such as a narrow bandgap of 1.2 eV with a p-type semiconductive characteristics, easy synthesis, low cost, and non-toxicity [8, 10–12], making it suitable for gas detection [13]. However, the p-n junction is the most effective structure in gas detection due to its high response; therefore, various structures of SnO_2 and CuO can be synthesized using different approaches, including sol-gel [14], atomic layer deposition (ALD) [15], hydrothermal synthesis [16, 17], electrospinning [8], precipitation [18], and microwave-assisted [19] techniques.

Microwave (MW) irradiation is a popular technique for synthesizing various materials, including organic and inorganic chemicals, which can be used in biochemical processes [20]. It is favored for its speed, time-saving capabilities, and low cost. This method operates without high pressure and temperature, yet it can produce nanostructured materials with uniform shape and size in nanoparticles [20–22]. Therefore, microwave irradiation is suitable for synthesizing a wide range of materials and offers an alternative way for producing metal oxide nanostructured materials. Microwave-assisted synthesis of SnO_2 and CuO materials has been reported. Wang et al. prepared Pt/SnO_2 nanostructures via a facile one-step microwave-assisted hydrothermal route in weight percentages of 1.5, 3, 4.5 wt.% for carbon monoxide (CO) gas sensors. The findings revealed that among them 3.0 wt.% Pt/SnO_2 showed the best performance for detecting 100 ppm carbon monoxide (CO) at 225 °C with response of 3 and response time of 16 s [23]. Pech-Rodríguez et al. synthesized SnO_2/CuO nanocomposites via a microwave-assisted polyol process. SnO_2/CuO heteronanostructures have been employed as effective electrocatalysts for hybrid water splitting. The results indicate that SnO_2/CuO heteronanostructures synthesized using a microwave-assisted polyol technique can be active for the assisted oxygen evolution reaction [19]. Moreover, Silva et al. prepared SnO_2: Zn nanocrystals synthesized via a microwave-assisted route and investigated their NO_2 gas-sensing properties. Gas sensing tests revealed that the zinc-doped SnO_2 nanoparticles were highly sensitive and exhibited good recovery and stability even under ambient humidity for NO_2 gas concentrations at sub-ppm levels at 150 °C [24].

Combining n-type SnO_2 with p-type CuO lowers the sensor's operating temperature and boosts VOC detection by forming a p-n junction, which widens the depletion region and improves charge transfer efficiency [25]. However, few studies report the synthesis of SnO_2/CuO composites using the same mass ratio of precursors. In addition, while the synthesis of composites with NaCl residues or other alkali halides on the surface has not been studied, their effects on SnO_2/CuO sensors have not yet been investigated. Therefore, addressing these issues, especially using halide-controlled stoichiometric microwave synthesis followed by long-term gas detection tests, is essential to move SnO_2/CuO VOC sensors from laboratory prototypes to reliable field devices.

This work depicts a low-cost, domestic microwave-assisted fabrication process for producing SnO_2/CuO heteronanostructures with NaCl residual. A single one-minute microwave treatment followed by calcination at 500 °C yields a three-phase composition consisting of SnO_2, CuO, and NaCl. The material shows a quick and selective ethanol response at RT, with strong sensor signals and rapid response and recovery times at 100 ppm, indicating its potential for scalable, reliable portable VOC sensors in ambient environments.

Materials and methods

Synthesis of SnO_2-NaCl nanoparticles

The SnO_2 nanoparticles were prepared using microwave-assisted synthesis. Firstly, 4 g of tin chloride dihydrate ($SnCl_2{\cdot}2H_2O$) powder was poured into a beaker and mixed with 20 mL of deionized water (DI water) and a dropwise addition of sodium hydroxide (NaOH) until the mixture reached a pH of 11 [26–28]. The solution was then stirred for another 60 min. After that, the product was placed in a microwave oven (Mitron, P70D17J-D3) using medium-low heat for 60 s. Followed by washing with DI water and ethanol using an ultrasonic cleaner. Subsequently, the formed SnO_2 was kept in an oven (OXYGEN, DN09D) to dry at 100 °C for 2 h, as shown in Fig. 1a.

SnO_2/CuO heteronanostructures with residual NaCl

For the SnO_2/CuO nanocomposite, 4 g of $SnCl_2{\cdot}2H_2O$ and 4 g of $CuSO_4{\cdot}2H_4O$ were co-dissolved in 20 mL DI water, adjusted to pH 11 with NaOH, and processed under the same conditions, yielding the SnO_2/CuO nanocomposite. The product was placed in a ceramic cup and annealed in a high-temperature muffle furnace at 500 °C for 2 h [26–29]. The schematic diagram illustrating the SnO_2-NaCl nanoparticles and SnO_2/CuO heteronanostructures with residual NaCl, as shown in Fig. 1a.

Fabrication of laser-induced graphene (LIG) device

The laser engraving process was carried out using a commercial CO_2 laser system (VLS 4.6/75, 10.6 μm) [1]. For the fabrication, we applied 25% of the maximum laser power, 30% of the maximum speed, and a resolution of 500 PPI to obtain low sheet resistance in the laser-induced graphene interdigitated electrodes (LIG-IDE), Fig. 1b. The LIG-IDE structure consisted of six interdigitated fingers, each with a spacing of 0.5 mm, a finger width of 0.5 mm, and a bus bar width of 1 mm on the collecting side.

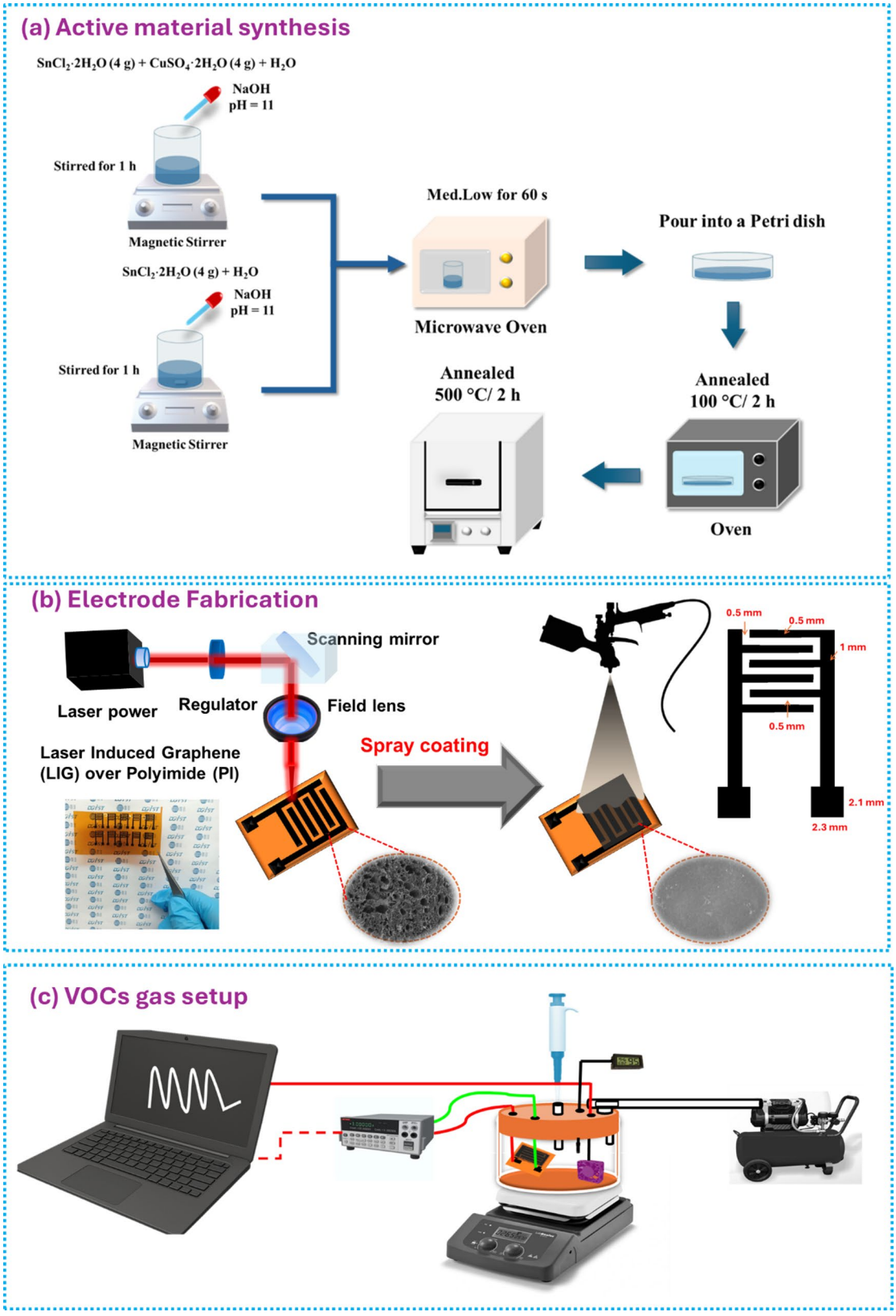

Fig. 1 **a** Schematic diagram illustrating the synthesis procedure of SnO_2-NaCl nanoparticles and SnO_2/CuO hetero-nanostructures with residual NaCl via a microwave-assisted method, followed by drying and calcination steps; **b** Fabrication of a laser-induced graphene interdigitated pattern and spray printing of SnO_2-CuO; and **c** VOCs gas setup

Ink formulation and spray coating

Pure SnO_2 and SnO_2-CuO inks were prepared at a concentration of 10 mg mL^{-1} in a 1:1 mixture of ethanol and isopropanol (EtOH: IPA), with 2 mg mL^{-1} of PVP, and sonicated for 10 min to enhance dispersion for spray coating [30]. The resulting ink was spray-deposited (500 µL) onto the LIG-IDE to precisely control the thickness and geometry of the film, as depicted in Fig. 1b. The active material was applied in a square pattern (5 mm × 5.5 mm) with a mass loading of 5 mg. A uniform coating was achieved by maintaining a consistent spray-to-substrate distance of 5 cm under an air pressure of 20 PSI. Finally, the sensor was annealed at 70 °C to remove residual solvents and moisture.

Characterization

The crystal structure of SnO_2-NaCl nanoparticles and SnO_2/CuO heteronanostructures with residual NaCl was analyzed by using an X-ray diffraction technique (Rigaku Mini Flex 600 instrument (M/S, Japan) with Cu-Kα (λ = 1.5405Å) with step size 3 degree/min. Then, SnO_2-NaCl nanoparticles and SnO_2/CuO hetero nanostructures with residual NaCl morphology were investigated using a Scanning Electron Microscope (SEM, SU-8230, Japan). Gas-sensing performance was evaluated using our mentioned design in Fig. 1c towards VOC gases at 30 ± 3 °C, connected to a Keithley 2400c source meter, USA. The system represents a VOC ethanol-sensing platform integrated with an airflow meter for controlled gas exchange and sensor recovery, enabling real-time electrical characterization. A sealed test chamber was placed on a hot plate to maintain the measurement temperature at 30 ± 3 °C, assisted by a fan to ensure uniform ethanol distribution. The chamber also contained humidity and temperature sensors, while the sensor device was positioned inside to maintain them at 10 RH% and 30 ± 3 °C during measurements. The source meter recorded the electrical response, allowing controlled evaluation of sensor performance under varying ethanol concentrations (20–100 ppm). VOC gases are introduced into the chamber via a micropipette through an injection port in volumes that were calculated by Eq. (1). The volume of high-purity alcohol (V) [99.99%] is calculated by the equation below using the desired gas concentration (in ppm) within the test chamber volume [31]. The sensor response (SR) was determined based on the electrical resistance in air (R_a) and the electrical resistance upon exposure to EtOH gas (R_g) using Eq. (2) [32–34]. The response time is the 90% of time needed for the sensor to react to reintroducing EtOH gas [33], while the recovery time represents the time needed for the sensor to return to 90% of its initial state when air gas is reintroduced [35, 36].

$$V = \frac{Cv_aM}{2.46 * 10^7 * D} \tag{1}$$

$$SR = \frac{R_a}{R_g} \qquad Reducing\ gases \tag{2}$$

where C and v_a are the desired gas concentration (ppm) and the volume of the test chamber (mL), respectively, while M and D are the molecular weight (g mol^{-1}) and the density of the desired alcohol (g mL^{-1}), respectively.

Results and discussion

Structural analysis

Figure 2 presents the X-ray diffraction (XRD) patterns of the investigated powders, revealing three principal crystalline phases: rutile-SnO_2, tenorite-CuO, and cubic NaCl. For the SnO_2-NaCl nanoparticles (red line), diffraction peaks appear at 2θ = 26.6°, 33.9°, 37.9°, 51.8°, and 55.0°, which can be indexed to the (110), (101), (200), (211), and (220) planes of rutile-SnO_2 (PDF 41-1445) [37]. Additional reflections at 31.7° and 45.5° correspond to the (111) and (200) planes of rock-salt NaCl (PDF 05-0628) [38]. The low intensity of these NaCl peaks, consistent with Wang et al. [39], indicates that only residual amounts of the salt remain after calcination at 500 °C. The SnO_2/CuO heteronanostructures with residual NaCl (black line) show the same SnO_2 and NaCl reflections together with new peaks at 32.5° (110), 35.5° (002), 38.7° (111), and 48.7° (202), assigned to tenorite-CuO (PDF 45-0937) [40, 41]. Their coexistence confirms the formation of a p-CuO/n-SnO_2 heterojunction within the nanocomposite, a junction type known to lower operating temperature and enhance ethanol sensing [25, 42].

Although the residual NaCl is present only in residual quantities, such alkali-halide layers can adsorb a thin film of moisture, accelerate the O_2/O_2^- surface exchange, and mitigate baseline drift under high relative humidity, as demonstrated for KCl- and NaCl-modified SnO_2/CuO systems [39, 43]. Taken together, these structural features render SnO_2/CuO-NaCl heteronanostructures highly suitable for low-temperature ethanol sensing, benefiting simultaneously from the p-n junction at SnO_2/CuO interfaces [44] and NaCl-templated porosity [45].

The SnO_2-NaCl nanoparticles shown in Fig. 3a consist of 20–40 nm nanocrystals interconnected into a highly porous foam. The broad SnO_2 peaks, along with the intense NaCl peaks (200, 220, 222), support the role of NaCl as a salt template. This template creates porosity and inhibits grain coarsening [45–47], and such microstructures are consistent with the excellent ethanol-sensing behavior of porous SnO_2 [48]. Figure 3b shows the surface of the SnO_2/CuO-NaCl heteronanostructures. This material forms large clusters, approximately 200–400 nm, which are themselves composed of

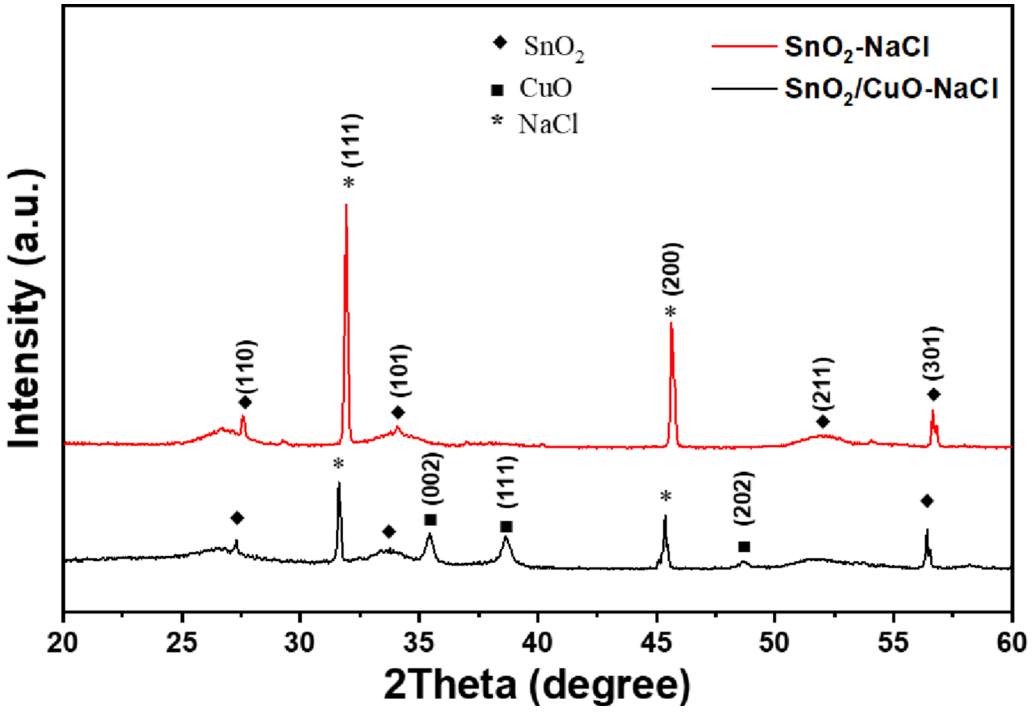

Fig. 2 XRD pattern of SnO_2-NaCl nanoparticles and SnO_2/CuO heteronanostructures with residual NaCl

smaller crystallites around 15 nm. The assembled XRD patterns display prominent CuO peaks alongside SnO_2 and residual NaCl. This indicates the independent crystallization of the two oxide phases and a high density of p-n junctions, a characteristic associated with fast ethanol response time [44]. Overall, the LIG crack network, the porosity created by NaCl, and the well-dispersed CuO on SnO_2 work together synergistically. This collective effect enlarges the specific surface area, increases oxygen adsorption sites [49, 50], and boosts the p-n junction density [51], thus enabling the composite samples to exhibit promising gas-sensing capabilities. Figure 3c shows the LIG-SnO_2/CuO-NaCl film, where 50–200 µm shrinkage cracks propagate through LIG layer. This forms a three-dimensional conductive network and creates openings for gas diffusion. The SnO_2/CuO nanoparticles deposited on the LIG match the XRD patterns, which show the SnO_2 (110, 101) and CuO (−111, 111) phases. This confirms the formation of p-n heterojunctions at the interface, a feature widely reported to accelerate chemiresistive reactions [52, 53]. Table 1 confirms the weight and atomic percentages of each element in SnO_2, SnO_2-CuO, and SnO_2-CuO/LIG.

VOCs sensing measurements

The gas sensing performance of 500 µL deposited pure SnO_2 and SnO_2-CuO, patterned in a square configuration on the LIG-IDE, was evaluated for ethanol detection. Figure 4a, b represents a comparative analysis of the ethanol sensing behavior of the pure SnO_2 and SnO_2-CuO sensors exposed sequentially to ethanol concentrations ranging from 100 to 20 ppm in dry air with RH 10% and 30 ± 3 °C. Pure SnO_2 sensors exhibited lower resistance than SnO_2-CuO, which is consistent with Zhou et al.'s work, as the increasing in CuO contents increases the resistance of SnO_2 [54]. As discussed by R.N. Mariammal et al. [55], apart from the formation of p–n junction, it is expected that doping of SnO_2 with Cu would enhance the oxygen vacancies, thus triggering the surface reactions. Pure SnO_2 and SnO_2-CuO sensors exhibited an n-type response trend toward ethanol, as evidenced by the decrease in resistance upon 60 s exposure to the reducing gas, attributed to electron donation. The sensor achieved a high response (R_{air}/R_{gas}) of 11 at 100 ppm, with fast response and recovery times of 53 s and 64 s, at RT, respectively. Figure 4c-d, compared to pure SnO_2 reported in literature, which achieved a response of 10.5 at 350 °C [56].

Moreover, Fig. 4e exhibited high lifetime stability over 30 days, which proves the capability of using the sensor in environmental real-time sensing. Figure 4f indicates the selectivity test over IPA, MeOH, and acetone towards ethanol at 100 ppm, which is important for real-time application to detect one gas over others with high selectivity and response. In SnO_2/CuO composite sensors, selectivity arises from the formation of a p-n heterojunction at the SnO_2 (n-type) and CuO (p-type) interface. This heterojunction affects the charge carrier

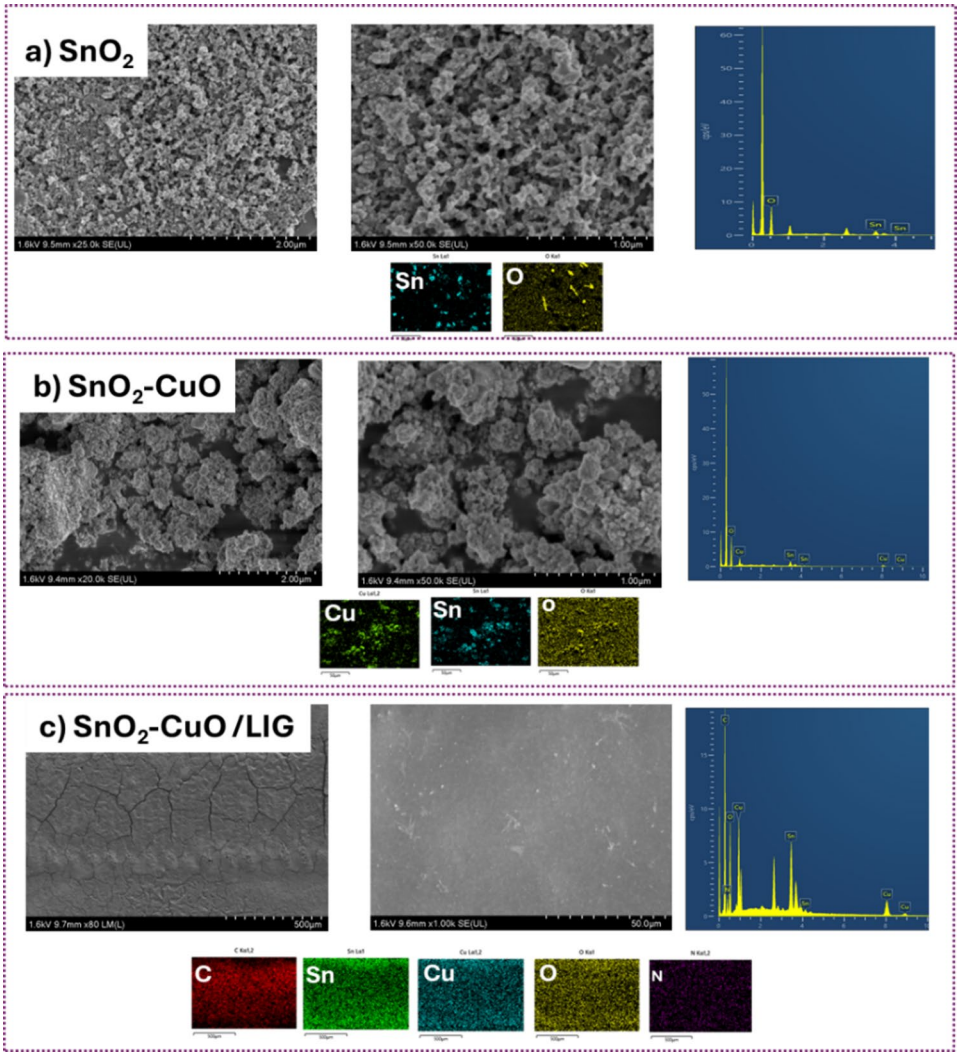

Fig. 3 SEM images and EDS of (**a**) SnO_2-NaCl nanoparticles with 20–40 nm grains; **b** SnO_2/CuO-NaCl heteronanostructures showing large clusters, approximately 200–400 nm; **c** LIG-SnO_2/CuO-NaCl film with 50–200 µm cracks in the laser-induced graphene

Table 1 EDS mapping elemental composition

Materials	Element	Wt.%	Atomic %
SnO_2	O	70.68	94.70
	Sn	29.32	5.30
	Total	100.00	100.00
SnO_2-CuO	O	50.97	84.25
	Cu	24.94	10.38
	Sn	24.08	5.37
	Total	100.00	100.00
SnO_2-CuO/LIG	C	32.05	57.36
	N	3.68	5.64
	O	19.35	26.01
	Cu	18.14	6.14
	Sn	26.79	4.85
	Total	100.00	100.00

depletion layer and resistance in specific ways, depending on the gas [57]. Figure 4g evaluates the cyclic stability of the sensor towards ethanol at 100 ppm through 10 cycles with an average response of 12.77. A consistent and reproducible decrease in resistance is observed with each gas pulse, followed by a clear recovery when ethanol is removed, indicating excellent reversibility and surface regeneration. Table 2 demonstrates the comparison between recent work and reported works in the literature. Figure 4h shows the ethanol sensing mechanism. The sensing mechanism involves the oxidation of ethanol molecules by chemisorbed oxygen (e.g., O_2^-) at RT, releasing electrons back into the conduction band and thereby reducing resistance [58, 59]. This highlights the robust redox dynamics between ethanol and surface-adsorbed oxygen species, where ethanol donates electrons, reducing the surface depletion layer (EDL). As discussed by Mariammal et al. [55], they found that the

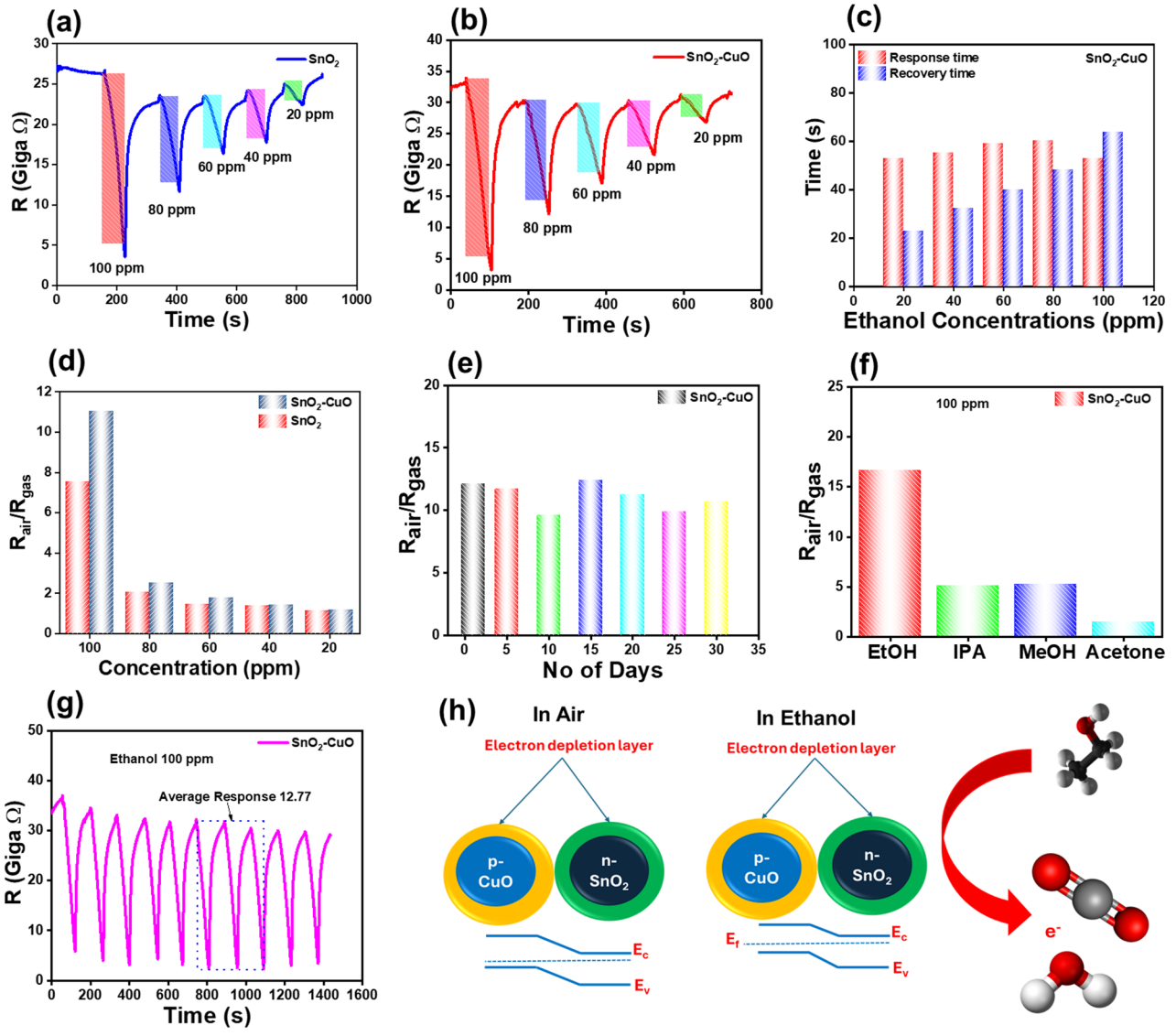

Fig. 4 Gas sensing performance of pure SnO_2 and SnO_2-CuO towards EtOH at RT: Gas sensing performance at different concentrations from 100 to 20 ppm of (**a**) pure SnO_2 and (**b**) SnO_2/CuO; **c** recovery and response times; **d** response versus concentrations; **e** lifetime stability at 100 ppm; **f** selectivity towards ethanol, IPA, MeOH, and acetone; **g** cyclic stability; and **h** ethanol sensing mechanism

Table 2 EtOH ethanol sensing performance compared to reported works in literature

Materials	EtOH (ppm)	Temp (°C)	Response $s_1 = (\Delta R/R_a) \times 100\%$ or $s_2 = R_g/R_a$ or R_a/R_g	Response/recovery time (s)	Refs.
SnO_2	100	RT	$S_2 = 7.5$	61.5/104	This work
SnO_2-CuO	100	RT	$S_2 = 11$	53/64	This work
Sm-$ZnFe_2O_4$ nanoparticles	40	300	S2 = 37.1	50/116	[61]
SnO2-CuO	100	320	S2 = 8	4/10	[44]
5% Fe-doped ZnO	50	125	S1 = 77.25	16/24	[62]
SnO2	100	350	S2 = 10.5	5/40	[56]
CuO	1000	220	S2 = 1.5	30/100	[63]
Fe_2O_3-Co_3O_4 composite	100	250	S2 = 26.2	–/–	[64]
α-Fe_2O_3 nanoparticles	100	150	S1 = 14.5	–/–	[65]
SnO_2 hollow spheres	40	75	S2 = 20.1	110/90	[66]
SnO_2 LA nanoparticles	40	150	S2 = 59.6	105/100	[66]
α-Fe_2O_3(0.09)/Nb_2O_5	100	160	S2 = 12.6	8/2	[67]

ethanol sensing mechanism in n-type MOS is governed by the interaction between ethanol molecules and chemisorbed oxygen species (O_2^-, O^{2-} and O^-) on the semiconductor surface. The reaction restores trapped electrons to the conduction band, reducing the depletion layer and increasing conductivity, which forms the basis for gas detection. As discussed by Abokifa et al. [60], they found confirmation by DFT about forming pre-adsorbed oxygen species at RT. Oxygen molecules from the ambient atmosphere first adsorb onto the metal oxide surface and become ionised into superoxide species (O_2^-) by capturing free electrons from the conduction band. At higher temperatures above 200 °C, these superoxide ions further transform into more reactive oxygen anions (O^- and O^{2-}) that trap free electrons, lowering the material's carrier concentration and conductivity. When the target gas reacts with these ionosorbed oxygen species, the trapped electrons are released, causing a distinct change in resistance that enables gas detection.

$$C_2H_5OH\ (gas)\ \rightarrow\ C_2H_5OH\ (ads) \quad (3)$$

$$C_2H_5OH\ (ads) + 3O_2^-\ (ads) \rightarrow\ 2CO_2 + 3H_2O + 3e^- \quad (4)$$

Conclusions

This study presented a comprehensive evaluation of pure SnO_2 and SnO_2/CuO nanostructures ethanol sensors fabricated using domestic microwave and annealing approaches, with extensive characterization via SEM, XRD, and gas sensing analysis. The sustainable synthesis route successfully produced SnO_2 and SnO_2/CuO nanostructures with favourable surface morphology and oxygen-rich active sites, enabling enhanced interaction with ethanol gas. The fabricated sensor demonstrated high sensor response at room temperature, along with high selectivity, fast response and recovery times, and prolonged operational stability. The SnO_2/CuO-based sensors achieved a response of 11 with response/recovery times of 53/64 s at 100 ppm of ethanol, indicating their strong potential for practical ethanol detection at RT.

Author contributions

Pitchanunt Chaiyo: Conceptualization, Writing-Original Draft, Mohamed Ahmed Belal: Investigation, Formal analysis, Writing-Original Draft, Sugato Hajra: Writing-Editing, Data Curation, Swati Panda: Writing-Editing, Visualisation, Premkumar Sharad Bhosale: Data Curation, Hohyun Keum: Funding Acquisition, Project administration, Visualisation, Hoe Joon Kim: Supervision, Funding Acquisition, Writing-Editing.

Funding

This research was supported by the National Research Foundation of Korea (NRF) (RS-2024-00346135). SH would like to thank the support of the InnoCORE program of the Ministry of Science and ICT (25-InnoCORE-01). We acknowledge the support from the Korea Institute of Industrial Technology as "Development of core technology for smart sensing and digital medical process to support medical surgical field diagnosis" (KITECH EH-25-0002).

Data availability

Data and materials are available upon request to the authors.

Declarations

Ethics approval and consent to participate

Not applicable.

Consent for publication

Not applicable.

Competing interests

The authors declare no competing interests.

Received: 5 October 2025 / Accepted: 16 November 2025
Published online: 23 December 2025

References

1. Belal MA, Hajra S, Panda S, Kaja KR, El-Moneim AA, Achary P. Ganga Raju, Kim HJ (2025) Mechanochemically synthesized ZIF-8@ZnO composite-based NO_2 gas detection. New J Chem 49(42):18436–18446. https://doi.org/10.1039/d5nj02514a
2. Belal MA, Panda S, Khanapuram U, Hajra S, Kaja KR, Rajaboina RK, Vivekanantha V, Vittayakorn N, Kim HJ (2025) Advances in nanogenerator enabled smart mask-based self-powered health monitoring units. Mater Adv 6(22):8210–8238. https://doi.org/10.1039/d5ma00845j
3. Belal MA, Hajra S, Panda S, Kaja KR, Park KJ, Jana R, Achary P. Ganga Raju, Kim HJ (2025) Functionalized MWCNTs@ZnO nanocomposites via spray printing for NO_2 gas sensing. J Mater Sci Mater Elec 36(12):750. https://doi.org/10.1007/s10854-025-14663-9
4. Li Z, Zeng W, Li Q (2022) SnO_2as a gas sensor in detection of volatile organic compounds: a review. Sens Actuators A Phys. https://doi.org/10.1016/j.sna.2022.113845
5. Belal MA, Hajra S, Panda S, Kaja KR, Abdo MMM, El-Moneim A. Abd, Janas D, Mishra YK, Kim HJ (2025) Advances in gas sensors using screen printing. Journal of Materials Chemistry A 13(8):5447–5497
6. Belal MA, Hajra S, Panda S, Kaja KR, Park KJ, Kim HJ (2025) Spray-printed ZnO thin film for high-sensitivity NO_2 gas sensing. Micro Nano Syst Lett 13(1):10
7. Taulo GT, Moharm AE, Belal MA, Shaalan NM, Ayad MM, Mohamed GG, El-Moneim AA (2025) Impact of NS co-doped rGO on the CO gas sensing performance of inkjet-printed SnO_2nanoparticles. Sens Actuators B Chem. https://doi.org/10.1016/j.snb.2025.138186
8. Zhang J, Ma S, Wang B, Pei S (2021) Preparation of composite SnO_2/CuO nanotubes by electrospinning and excellent gas selectivity to ethanol. Sens Actuators A Phys. https://doi.org/10.1016/j.sna.2021.113090
9. Kang X, Deng N, Yan Z, Pan Y, Sun W, Zhang Y (2022) Resistive-type vocs and pollution gases sensor based on SnO_2: a review. Mater Sci Semicond Process. https://doi.org/10.1016/j.mssp.2021.106246
10. Phuoc PH, Hung CM, Toan N. Van, Duy N. Van, Hoa ND, Hieu N. Van (2020) One-step fabrication of SnO_2porous nanofiber gas sensors for sub-ppm H_2S detection. Sens Actuators A Phys. https://doi.org/10.1016/j.sna.2019.111722
11. Kadhim IH, Hassan HA, Ibrahim FT (2020) Hydrogen gas sensing based on nanocrystalline SnO_2 thin films operating at low temperatures. Int J Hydrogen Energy 45(46):25599–25607. https://doi.org/10.1016/j.ijhydene.2020.06.136
12. Choi M. Sik, Ahn J, Kim M. Young, Mirzaei A, Choi S-M, Chun D. Won, Jin C, Lee K. Hyoung (2021) Changes in the crystal structure of SnO_2nanoparticles and improved H_2S gas-sensing characteristics by al doping. Appl Surf Sci. https://doi.org/10.1016/j.apsusc.2021.150493
13. Tian Z, Bai H, Li Y, Liu W, Li J, Kong Q, Xi G (2020) Gas-sensing activity of amorphous copper oxide porous nanosheets. ChemistryOpen 9(1):80–86. https://doi.org/10.1002/open.201900327
14. Poiasina MP, Bianchetti MF, Bojorge CD, Gard FS (2025) Characterization of cuo-doped SnO_2 thin films prepared by sol–gel and dip-coating: a multi-analytical approach. Surf Interface Anal 57(8):600–618. https://doi.org/10.1002/sia.7418
15. Li S, Li X, Guo J, Liu X, Zhang J (2025) Heterostructured SnO_2/CuO hydrangea nanocomposites for highly sensitive NO_2 detection. ACS Appl Nano Mater 8(20):10549–10558. https://doi.org/10.1021/acsanm.5c01293

16. Al-Mousawi RA, Al-Kadhemy MFH, Abbas KN, Saeed AA (2024) Activity SnO_2/CuO nanocomposite toward photocatalytic degradation of methylene blue dye under solar light. AIP Conf Proc. 3097(1):090020
17. Taulo GT, Shaalan NM, Mohamed GG, Ayad MM, El-Moneim AA (2024) Inkjet printing of SnO_2 nanoparticles with exposed high-energy facets for Co gas sensing. Ceram Int 50(11):18638–18646. https://doi.org/10.1016/j.ceramint.2024.02.352
18. Dhage SB, Patil VL, Patil PS, Ryu J, Patil DR, Malghe YS (2021) Synthesis and characterization of CuO-SnO_2nanocomposite for CO gas sensing application. Mater Lett. https://doi.org/10.1016/j.matlet.2021.130831
19. Pech-Rodríguez WJ, García-Lezama HM, Sahin NE (2023) Facile preparation of SnO_2/CuO nanocomposites as electrocatalysts for energy-efficient hybrid water electrolysis in the presence of ethanol. Energies. https://doi.org/10.3390/en16134986
20. Devi N, Sahoo S, Kumar R, Singh RK (2021) A review of the microwave-assisted synthesis of carbon nanomaterials, metal oxides/hydroxides and their composites for energy storage applications. Nanoscale 13(27):11679–11711. https://doi.org/10.1039/d1nr01134k
21. Kang S, Mirzaei A, Shin KY, Oum W, Yu DJ, Kim SS, Kim HW (2023) Highly selective NO_2 gas sensing with SnO_2-Ti_3C_2T nanocomposites synthesized via the microwave process. Sens Actuators B Chem. https://doi.org/10.1016/j.snb.2022.132882
22. Gaber A, Attia SY, Salem AMS, Mohamed SG, El-Hout SI (2023) Microwave-assisted fabrication of SnO_2nanostructures as electrode for high-performance pseudocapacitors. J Energy Storage. https://doi.org/10.1016/j.est.2022.106358
23. Wang Q, Bao L, Cao Z, Li C, Li X, Liu F, Sun P, Lu G (2020) Microwave-assisted hydrothermal synthesis of Pt/SnO_2 gas sensor for CO detection. Chin Chem Lett 31(8):2029–2032. https://doi.org/10.1016/j.cclet.2019.12.007
24. da Silva LF, Lucchini MA, Catto AC, Avansi W Jr., Bernardini S, Aguir K, Niederberger M, Longo E (2023) The role of Zn ions in the structural, surface, and gas-sensing properties of SnO_2:Zn nanocrystals synthesized via a microwave-assisted route. Sensors (Basel). https://doi.org/10.3390/s24010140
25. Paleczek A, Szafraniak B, Fusnik L, Brudnik A, Grochala D, Kluska S, Jurzecka-Szymacha M, Maciak E, Kaluzynski P, Rydosz A (2021) The heterostructures of CuO and SnO_X for NO_2 detection. Sensors (Basel). https://doi.org/10.3390/s21134387
26. Stefan M, Leostean C, Pana O, Popa A, Toloman D, Macavei S, Perhaita I, Barbu-Tudoran L, Silipas D (2019) Interface tailoring of SnO_2–TiO_2 photocatalysts modified with anionic/cationic surfactants. J Mater Sci 55(8):3279–3298. https://doi.org/10.1007/s10853-019-04192-2
27. Sukriti P, Chand (2019) Effect of ph values on the structural, optical and electrical properties of SnO_2 nanostructures. Optik 181:768–778. https://doi.org/10.1016/j.ijleo.2018.10.203
28. Mamakhel A, Søndergaard M, Borup K, Brummerstedt Iversen B (2020) Continuous flow hydrothermal synthesis of rutile SnO_2nanoparticles: exploration of pH and temperature effects. J Supercrit Fluids. https://doi.org/10.1016/j.supflu.2020.105029
29. Van Viet P, Nguyen H-P, Tran H-H, Bui D-P, Hai LV, Pham M-T, You S-J (2021) Thi. Constructing g-C_3N_4/SnO_2 s-scheme heterojunctions for efficient photocatalytic no removal and low NO_2 generation. J Science: Adv Mater Devices 6(4):551–559. https://doi.org/10.1016/j.jsamd.2021.07.005
30. Ma HZ, Luo C, Zhao JN, Shao Y, Zhang YH, Liu X, Li S, Yin B, Zhang K, Ke K, Zhou L, Yang MB (2023) Metal-organic framework based triboelectric nanogenerator for a self-powered methanol sensor with high sensitivity and selectivity. ACS Appl Mater Interfaces 15(31):37563–37570. https://doi.org/10.1021/acsami.3c07966
31. Parayil RT, Bhagat B, Gupta SK, Mukherjee K, Mohapatra M (2024) Oxygen vacancy-enriched $Zn_2SnO_4$for aliphatic alcohol sensing and enhanced selectivity towards n-butanol. Phys Chem Chem Phys 26(9):7424–7434. https://doi.org/10.1039/d3cp05178a
32. Birajdar SN, Adhyapak PV (2020) Palladium-decorated vanadium pentoxide as nox gas sensor. Ceram Int 46(17):27381–27393. https://doi.org/10.1016/j.ceramint.2020.07.223
33. Me DM, Sundaram NG, Singh A, Singh AK, Kalidindi SB (2019) An amine functionalized zirconium metal-organic framework as an effective chemiresistive sensor for acidic gases. Chem Commun (Camb) 55(3):349–352. https://doi.org/10.1039/c8cc06875e
34. Liu X-L, Ma S-X, Zhu S-W, Zhao Y, Ning X-J, Zhao L, Zhuang J (2019) Light stimulated and regulated gas sensing ability for ammonia using sulfur-hyperdoped silicon. Sens Actuators B 291:345–353. https://doi.org/10.1016/j.snb.2019.04.073
35. Park JY, Kwak Y, Lim HR, Park SW, Lim MS, Cho HB, Myung NV, Choa YH (2022) Tuning the sensing responses towards room-temperature hypersensitive methanol gas sensor using exfoliated graphene-enhanced ZnO quantum dot nanostructures. J Hazard Mater 438:129412. https://doi.org/10.1016/j.jhazmat.2022.129412
36. Jaiswal J, Singh P, Chandra R (2021) Low-temperature highly selective and sensitive NO_2gas sensors using cdte-functionalized ZnO filled porous Si hybrid hierarchical nanostructured thin films. Sens Actuators B Chem. https://doi.org/10.1016/j.snb.2020.128862
37. Doubi Y, Hartiti B, Batan A, Siadat M, Labrim H, Tahiri M, Kotbi A, Thevenin P, Jouiad M (2025) Controlled SnO_2nanostructures for enhanced sensing of hydrogen sulfide and nitrogen dioxide. Sens Actuators B Chem. https://doi.org/10.1016/j.snb.2025.137878
38. Yuan C, Wu W-W, Liu Y, Wang Z, Yang Y, Han L-L, Zhou Q, Liu J-Q, Liu P (2022) High yield hollow carbon cubes with excellent microwave absorption property at a low loading ratio. Carbon 195:101–111. https://doi.org/10.1016/j.carbon.2022.04.007
39. Wang L, Huang F, Yao X, Yuan S, Yu X, Tu ST, Chen S (2023) Collaborative enhancement of humidity sensing performance by kcl-doped CuO/SnO_2p-n heterostructures for monitoring human activities. ACS Omega 8(5):4878–4888. https://doi.org/10.1021/acsomega.2c07098
40. Ni Z, Wan M, Tang G, Sun L (2022) Synthesis of cuo and paa-regulated silver-carried CuO nanosheet composites and their antibacterial properties. Polymers (Basel). https://doi.org/10.3390/polym14245422
41. Zhou J, Gao Q, Zhang Y, Shao Z, Zhang N, Qin Y, Feng W (2024) CuO nanobelt array-based omnidirectional uv-visible-nir photoelectrochemical photodetectors. ACS Appl Mater Interfaces 16(51):70694–70700. https://doi.org/10.1021/acsami.4c17080
42. Ayesh AI, Alyafei AA, Anjum RS, Mohamed RM, Abuharb MB, Salah B, El-Muraikhi M (2019) Production of sensitive gas sensors using CuO/SnO_2nanoparticles. Appl Phys A. https://doi.org/10.1007/s00339-019-2856-6
43. Song X, Qi Q, Zhang T, Wang C (2009) A humidity sensor based on kcl-doped SnO_2 nanofibers. Sens Actuators B Chem 138(1):368–373. https://doi.org/10.1016/j.snb.2009.02.027
44. Zhang J, Ma S, Wang B, Pei S (2021) Hydrothermal synthesis of SnO_2-CuO composite nanoparticles as a fast-response ethanol gas sensor. J Alloys Compd. https://doi.org/10.1016/j.jallcom.2021.161299
45. Shu Y, Liu Q, Shi M, Zhang Z, Xie C, Bi S, Zhang P (2024) Surfactant-free synthesis of crystalline mesoporous metal oxides by a seeds/ nacl-mediated growth strategy. Adv Sci Weinh 11(1):e2304533. https://doi.org/10.1002/advs.202304533
46. Shu Y, Chen H, Chen N, Duan X, Zhang P, Yang S, Bao Z, Wu Z, Dai S (2020) A principle for highly active metal oxide catalysts via NaCl-based solid solution. Chem 6(7):1723–1741. https://doi.org/10.1016/j.chempr.2020.04.003
47. Amer MS, AlOraij HA, Al-Mayouf AM (2024) Facial synthesis of high-performance ni doped-tin oxide mesoporous for CO_2electroreduction to formate. Journal of CO2Utilization. https://doi.org/10.1016/j.jcou.2024.102742
48. Li G, Hou J, Hilal M, Kim H, Chen Z, Cui Y, Kim JH, Cai Z (2024) Development of high-performance ethanol gas sensors based on La_2O_3nanoparticles-embedded porous SnO_2nanofibers. Sensors. https://doi.org/10.3390/s24216839
49. Francis C, Rektor A, Valayil-Varghese T, McKibben N, Estrada I, Forbey J, Estrada D (2024) Laser-induced graphene gas sensors for environmental monitoring. Front Chem 12:1448205. https://doi.org/10.3389/fchem.2024.1448205
50. Zhang R, Yao Y, Lin G, Zhang X (2024) A flexible sensor fabricated by laser-induced graphene on PI fabric with macroscopic crack array for GF modulation strategy. Sens Actuators A Phys. https://doi.org/10.1016/j.sna.2024.115529
51. Sharma A, Eadi SB, Noothalapati H, Otyepka M, Lee HD, Jayaramulu K (2024) Porous materials as effective chemiresistive gas sensors. Chem Soc Rev 53(5):2530–2577. https://doi.org/10.1039/d2cs00761d
52. Ma S, Xu J (2023) Nanostructured metal oxide heterojunctions for chemiresistive gas sensors. J Mater Chem A 11(44):23742–23771. https://doi.org/10.1039/d3ta04953a
53. Yang S, Lei G, Xu H, Lan Z, Wang Z, Gu H (2021) Metal oxide based heterojunctions for gas sensors: a review. Nanomaterials (Basel). https://doi.org/10.3390/nano11041026
54. Zhou X, Cao Q, Huang H, Yang P, Hu Y (2003) Study on sensing mechanism of CuO–SnO_2 gas sensors. Mater Sci Eng B Solid-State Mater Adv Technol 99(1–3):44–47. https://doi.org/10.1016/s0921-5107(02)00501-9
55. Mariammal RN, Ramachandran K, Renganathan B, Sastikumar D (2012) On the enhancement of ethanol sensing by cuo modified SnO_2 nanoparticles

using fiber-optic sensor. Sens Actuators B Chem 169:199–207. https://doi.org/10.1016/j.snb.2012.04.067
56. Wang B, Sun L, Wang Y (2018) Template-free synthesis of nanosheets-assembled SnO_2hollow spheres for enhanced ethanol gas sensing. Mater Lett 218:290–294. https://doi.org/10.1016/j.matlet.2018.02.003
57. Ingole SM, Molane AC, Patel UJ, Patil SL, Selvaraj M, Assiri MA, Mahanwar PA, Patil VB (2025) Development of SnO_2/CuO heterostructure sensor for detection of toxic NO_2gas. Inorg Chem Commun. https://doi.org/10.1016/j.inoche.2025.115402
58. Tagbo PC, Mohamed MM, Ayad MM, El-Moniem AA (2025) Fabrication of flexible MoS_2sensors for high-performance detection of ethanol vapor at room temperature. Sens Actuators A Phys. https://doi.org/10.1016/j.sna.2025.116531
59. Thomas A, Thirumalaisamy L, Madanagurusamy S, Sivaperuman K (2023) Incompatibility of pure SnO_2 thin films for room-temperature gas sensing application. ACS Omega 8(36):32848–32854. https://doi.org/10.1021/acsomega.3c04038
60. Abokifa AA, Haddad K, Raman B, Fortner J, Biswas P (2021) Room temperature gas sensing mechanism of SnO_2towards chloroform: comparing first principles calculations with sensing experiments. Appl Surf Sci. https://doi.org/10.1016/j.apsusc.2021.149603
61. Khurshid R, Ali F, Afzal A, Ali Z, Qureshi MT (2019) Polyol-mediated coprecipitation and aminosilane grafting of superparamagnetic, spinel $ZnFe_2O_4$ nanoparticles for room-temperature ethanol sensors. J Electrochem Soc 166(4):B258–B265. https://doi.org/10.1149/2.1021904jes
62. Chandak VS, Kathwate LH, Kumbhar MB, Kulal PM (2025) Spray deposited high performance fe-doped ZnO ethanol sensor operating at low temperatures. J Ind Eng Chem 149:397–411. https://doi.org/10.1016/j.jiec.2025.01.053
63. Raksa P, Gardchareon A, Chairuangsri T, Mangkorntong P, Mangkorntong N, Choopun S (2009) Ethanol sensing properties of CuO nanowires prepared by an oxidation reaction. Ceram Int 35(2):649–652. https://doi.org/10.1016/j.ceramint.2008.01.028
64. Bagherzadeh Enferadi SMH, Mirzaei A (2024) Fe_2O_3-Co_3O_4 nanocomposite gas sensor for ethanol sensing studies. Ceram Int 50(24):52861–52870. https://doi.org/10.1016/j.ceramint.2024.10.138
65. Shoorangiz M, Shariatifard L, Roshan H, Mirzaei A (2021) Selective ethanol sensor based on α-Fe_2O_3nanoparticles. Inorg Chem Commun. https://doi.org/10.1016/j.inoche.2021.108961
66. Motsoeneng RG, Kortidis I, Ray SS, Motaung DE (2019) Designing SnO_2 nanostructure-based sensors with tailored selectivity toward propanol and ethanol vapors. ACS Omega 4(9):13696–13709. https://doi.org/10.1021/acsomega.9b01079
67. Khatoon R, Rauf S, Haq MU, Attique S, Din SU, Ali N, Guo Y, Chen H, Tian Y, Lu J (2021) Design of highly sensitive and selective ethanol sensor based on α-Fe_2O_3/Nb_2O_5 heterostructure. Nanotechnology 32(19):195503. https://doi.org/10.1088/1361-6528/abdd5e

Publisher's note